

Article

Fiber Jamming of Magnetorheological Elastomers as a Technique for the Stiffening of Soft Robots

Taylan Atakuru ^{1,*}, Fatih Kocabaş ¹, Niccolò Pagliarani ^{2,3}, Matteo Cianchetti ^{2,3} and Evren Samur ¹

¹ Department of Mechanical Engineering, Boğaziçi University, Istanbul 34342, Turkey; fatih.kocabas@boun.edu.tr (F.K.); evren.samur@boun.edu.tr (E.S.)

² The BioRobotics Institute, Scuola Superiore Sant'Anna, 56025 Pisa, Italy; niccolo.pagliarani@santannapisa.it (N.P.); matteo.cianchetti@santannapisa.it (M.C.)

³ Department of Excellence in Robotics and AI, Scuola Superiore Sant'Anna, 56127 Pisa, Italy

* Correspondence: taylanatakuru@gmail.com; Tel.: +90-543-320-2226

Abstract: There has been a notable focus on the adoption of jamming-based technologies, which involve increasing the friction between grains, layers, or fibers to achieve variable stiffness capability in soft robots. Additionally, magnetorheological elastomers (MREs) that show magnetic-field-dependent viscoelasticity have great potential as a material for varying stiffness. This study proposes a hybrid method (magnetic jamming of MRE fibers) for enhancing the stiffness of soft robots, combining a jamming-based with a viscosity-based method. First, a fiber jamming structure is developed and integrated into a soft robot, the STIFF-FLOP manipulator, to prove the concept of the magnetic jamming of MRE fibers. Then, based on the proposed method, a variable stiffness device actuated by electro-permanent magnets is developed. The device is integrated into the same manipulator and the electronically controlled magnetic jamming and stiffening of the manipulator is demonstrated. The experimental results show that stiffness gain in bending and compression is achieved with the proposed method. The outcomes of this investigation demonstrate that the proposed hybrid stiffening technique presents a promising avenue for realizing variable and controllable stiffness in soft robots.

Keywords: variable stiffness; fiber jamming; magnetic jamming; magnetorheological elastomer; electro-permanent magnet; soft robotics



Citation: Atakuru, T.; Kocabaş, F.; Pagliarani, N.; Cianchetti, M.; Samur, E. Fiber Jamming of Magnetorheological Elastomers as a Technique for the Stiffening of Soft Robots. *Robotics* **2024**, *13*, 16. <https://doi.org/10.3390/robotics13010016>

Academic Editors: Po-Yen Chen and Kean Aw

Received: 30 November 2023

Revised: 20 December 2023

Accepted: 26 December 2023

Published: 17 January 2024



Copyright: © 2024 by the authors. Licensee MDPI, Basel, Switzerland. This article is an open access article distributed under the terms and conditions of the Creative Commons Attribution (CC BY) license (<https://creativecommons.org/licenses/by/4.0/>).

1. Introduction

The demand for developing soft robots with high deformability and compliance has led to a growing interest in utilizing unconventional materials and structures [1,2]. Although a high degree of deformability and compliance is desirable, the stiffness of a soft robot must be in a delicate balance: it should be rigid and precise enough to exert significant force on its environment and perform tasks accurately, yet compliant enough to adapt to its environment. Achieving the ability to vary and control stiffness is still a major concern in soft robotics [3].

Various variable stiffness technologies have been used to achieve stiffness variation in soft robots [3]. These technologies fall into two main categories based on their use of active and semi-active elements. Active elements, like electroactive polymers [4], flexible fluidic actuators (FFAs) [5], and tendon-driven actuators [6], are used antagonistically and in combination with passive structures [7]. Additionally, semi-active elements (e.g., low melting point materials [8], shape-memory materials [9], viscosity-based materials, and jamming-based materials) are used to achieve variable stiffness. Alternatively, the stiffening of soft robotic structures is achieved through structural optimization. Childs and Rocker [10] introduced a rhombus-patterned backbone structure made of thin-walled plates, demonstrating a shear and torsional stiffness increase while permitting bending. Sun et al. [11] utilized 3D topology optimization to achieve multi-axis designs for flexure joints, enhancing the torsional stiffness of the structure. Among them, the concept of jamming transition

stands out as one of the most widely embraced due to its scalability, ease of fabrication, and cost-effectiveness [12]. Liu and Nagel [13] initially introduced the concept of jamming. Later, it has been described as frictional interactions by nearest-neighbor jamming particles [14,15]. In other words, an increase in relative shear stress between the particles results in a phase change in the structure. This change is generally supplied by external pressure. The structure is in the unjammed state (compliant) in the absence of pressure; whereas, it is in the jammed (stiff) state when uniform pressure is applied. Thus, the structure makes a transition from a compliant state to a rigid state.

Jamming can be induced through various mechanisms, including mechanical, electrostatic, magnetic, and pneumatic [16]. High directional pressure can be applied by mechanical actuation methods, such as clamps [17], cables [18,19], and meshes [20]. However, they require mechanical actuators, which may complicate system integration depending on the application field. Electrostatic [21,22] and magnetic jamming [23,24] methods also provide directional pressures; however, the applied pressure decreases as the distance between the charged or magnetized surfaces increases. Moreover, high voltages are essential, potentially limiting their application in safety-sensitive scenarios. In pneumatic jamming, using a vacuum is practical as it can maintain a uniform isotropic pressure within a jamming structure. However, it has several drawbacks. First, it requires a pump and an external membrane, which can make system integration difficult. Ensuring an effective seal for the membrane enclosing the stacked elements without restricting the movement of the structure is essential. Second, a ceiling exists for the maximum vacuum pressure achievable within the enclosing structure, particularly when reaching a perfect vacuum state. This limitation results in an applied pressure equivalent to the atmospheric pressure, thus restricting the range of slip thresholds the structure can attain. Third, the speed of this technology, which operates in seconds, is not remarkable, particularly the prolonged duration needed for the transition from a rigid state to a soft state [3].

Jamming structures have employed elements with diverse shapes and configurations, including grains, layers, and fibers. Granular jamming involves granular elements in an airtight envelope. In the absence of pressure, the grains can move freely with respect to each other; whereas, they are constrained when pressure is applied. Manti et al. [16] reported that granular jamming structures demonstrated stiffness changes (up to 40:1), which makes them well suited for robotic applications, such as soft grippers [25,26], manipulators [27–29], and haptic interfaces [30]. However, the application of granular jamming in soft devices presents certain disadvantages, including the displacement of granular materials during activation and the unpredictable system behavior. Layer jamming consists of compliant sheets instead of granules. The stiffness is modified using the friction between the layers [31]. It has several advantages over granular jamming. It offers a stiffness increase without a substantial change in volume, potentially more compact designs, and precise stiffness control. In addition, it can provide better stiffness variation because the increased contact area between the overlapping layers results in a higher friction force. A remarkable bending stiffness ratio (1800:1) is achieved through the utilization of layer jamming in the literature [32]. However, this substantial improvement is applicable only in one direction, which poses a notable challenge for soft robotic applications. On the other hand, fiber jamming emerges as a promising option among the jamming technologies. It is composed of longitudinal fibers. The fibers can rearrange like grains along one plane; whereas, they slide with respect to each other like layers on the two other orthogonal planes. This property makes fiber jamming very useful in applications in which variable bending stiffness in more than one direction is needed. Brancadoro et al. [33] pioneered the use of fibers as filler material to achieve jamming. Later, they demonstrated the applicability of fiber jamming technology in a minimally invasive surgery (MIS) manipulator [34]. Recently, Arleo et al. [35] developed a stiffness tunable actuator utilizing the fiber jamming principle. They have achieved a stiffness ratio of up to 21.3:1.

Magnetorheological (MR) materials, i.e., magnetorheological elastomers (MREs) and magnetorheological fluids (MRFs), belong to the category of smart materials whose stiffness

is modulated when exposed to a magnetic field. They are composed of magnetic-field-sensitive particles distributed or aligned in a specific direction within an elastomer or a fluid. These particles exhibit a MR effect when exposed to a magnetic field, resulting in a field-dependent property for the material, including a modifiable modulus and damping. This property is no longer present in the material in the absence of a magnetic field. Early work on MR materials [36–39] examined the changes in storage modulus and developed corresponding theoretical models for the behavior of elastomeric polymer materials with ferrous particles under a magnetic field. Since the early 2000s, there has been a remarkable increase in interest in MREs and their stiffening behavior [40–42]. For example, Schubert [43] performed several large-strain experiments with and without magnetic fields to characterize MREs. He developed constitutive models that capture the behavior of MREs using experimental data.

MR materials hold great promise for soft robotics because they allow rapid stiffness changes within milliseconds [44,45]. For instance, McDonald et al. [46] developed a valve utilizing MRFs for flow control in soft robots. Later, they [47] utilized electro-permanent magnets (EPMs) to modify the material properties of MRFs, enabling the regulation of pressure within soft actuators. An EPM is a solid-state device whose external magnetic flux can be stably switched on and off by a discrete electrical pulse. This makes an EPM a more desirable magnetic field source than an electromagnet since the energy is consumed only during the switching between the states and the transition can be controlled electronically. Gaeta et al. [24] introduced a magnetically controlled stiffening technique utilizing MRFs and jamming-based stiffening methods with the assistance of EPMs. However, challenges, such as particle settling and control difficulties, limit the use of MRFs. MREs address these issues associated with MRF applications [45,48]. The use of MREs in soft robotics is reviewed in [49], which highlights several applications of MREs, such as magnetostriction-based actuators [50], micro-actuators capable of rotation [51], pneumatic valves [52], soft inchworm robots [53,54], and soft skin sensors [55]. Furthermore, the article presents an illustrative case of a surgical manipulator with variable stiffness [56], which employs MREs and electromagnets within the design of a soft robot. MREs stand out in their effectiveness in terms of the speed of stiffening and destiffening (in milliseconds) and offer versatility in different modes of stiffening, such as bending, tension, and compression. However, achieving high stiffness variation requires the application of very strong magnetic fields.

In this paper, we present a new variable stiffness device for soft robots that exploits the fiber jamming technology and the variable viscoelastic behavior of MREs. The device employs magnetic jamming of MRE fibers to achieve increased stiffness variation, accomplished through a single magnetic actuation powered by electro-permanent magnets. Both jamming and viscoelasticity modification are achieved by this actuation. We implement this novel hybrid approach on a soft robot, the STIFF-FLOP surgical manipulator [57,58]. To demonstrate the concept of magnetic jamming of MRE fibers, a fiber jamming structure is initially developed and incorporated into the soft manipulator. Various experiments are carried out with this proof-of-concept test setup to investigate the stiffness alteration resulting from the jamming and variable viscoelasticity of MRE fibers. Finally, this paper exhibits the stiffening of the manipulator through electronically controlled magnetic jamming using the variable stiffness device.

2. Variable Stiffness Device Based on Magnetic Fiber Jamming

2.1. Design

The proposed variable stiffness device comprises MRE fibers and electro-permanent magnets (EPMs) designed to be incorporated into the STIFF-FLOP manipulator (see Figure 1). The MRE fibers are axially packed within the stiffening chamber of the manipulator. The geometry of the stiffening chamber is configured in a hexagonal shape, allowing for the highest packing density achievable for circles. The main reason to use the MRE fibers is to benefit from both the viscoelasticity change in MREs under a magnetic field (MR effect) and the increase in magnetic jamming force (jamming effect).

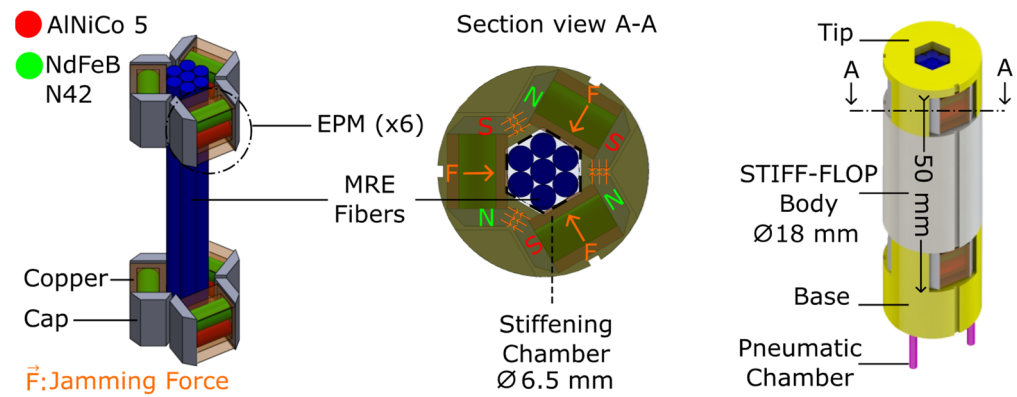


Figure 1. Conceptual design of the variable stiffness device. (Left) CAD drawing of the stiffening device. (Middle) A cross-sectional view indicating the magnetic polarity of the EPMs and explaining the jamming principle. (Right) The variable stiffness device is integrated into the STIFF-FLOP manipulator.

Six EPMs are used to induce the jamming of the fibers. Each EPM is composed of two permanent magnets with identical retentivity but differing coercivity, along with two iron caps and a coil system. The operational principle of an EPM device is detailed in Appendix A, providing energy consumption calculations. The EPMs are placed at the bottom and top areas of the manipulator in a way that they can move freely in the radial direction. They have two functions, which are to clamp the MRE fibers and create magnetic fields to make the MREs stiffer. The MRE fibers are positioned between the EPM caps. When the EPM is in its ON state, it generates a substantial magnetic field in that region, facilitating the MR effect. In addition, the identical EPMs with opposing magnetic poles on their facing caps create clamping forces for the jamming effect. The orientation of the EPMs is configured so that the proximal caps of two adjacent EPMs possess different polarization. This orientation is achieved when the polarity of a hard magnet pair forms a 120-degree angle. The tips of the iron caps that are facing each other are trimmed in such a way that the surface normals aligned in the same direction. This modification enhances the magnetic and jamming force generated. The EPMs are radially oriented around the central axis of the manipulator in a manner that allows copper wires to make tangential contact with the fibers. When the EPMs are activated, a significant magnetic force is generated between the facing caps of the EPMs (see Videos S1 and S3). This force exponentially increases as the caps approach each other. Consequently, the EPMs clamp the fibers, enabling jamming, and provide the necessary magnetic field, stiffening the MREs. This results in the manipulator becoming stiffer due to both factors: the jamming and MR effects.

According to the Euler–Bernoulli beam theory, the bending stiffness depends on E (Young’s moduli) and I (area moment of inertia). The theoretical prediction of the bending stiffness for the fiber jamming structure, which comprises circular fibers arranged in a hexagonal configuration, can be approximated by evaluating the area moment of inertia of the resulting hexagon (assuming no gaps between the fibers) [16]. Consequently, this estimation could help predict the change in stiffness during jamming. The area moment of inertia during the pre-slip region would be:

$$I_{pre\ slip} = \frac{5\sqrt{3}N^2d_f^4}{144} \tag{1}$$

where N is the number of fibers and d_f is the diameter of the fibers. The area moment of the inertia of a hexagon would be:

$$I_{slip} = \frac{\pi N d_f^4}{64} \tag{2}$$

which leads to a stiffness change of $1.23 N$.

A soft manipulator structure designed for MIS offers several advantages. It enhances dexterity and allows for a gentle interaction with soft tissue, thereby reducing the risk of injury to healthy tissue. The STIFF-FLOP manipulator is made up of a cylindrical elastomer, including a main body, a base, and a tip. It has three pneumatic chambers and a central channel that can perform certain tasks, such as carrying camera cables if mounted or a different implementation of a stiffness modulation mechanism or system. The kinematic model of the STIFF-FLOP manipulator is detailed in [58]. FFAs are used to actuate the three chambers, enabling the manipulator to squeeze and elongate without being damaged and perform omnidirectional bending.

The transition of the state of the EPMS between the “ON” and “OFF” states requires a current for a short period of time. Moreover, it is essential to have the capability to reverse the current direction to change the polarity of the soft magnet. This functionality can be accomplished through a motor driver and a microcontroller. Utilizing a single power supply and a motor driver for each EPM enables precise control over the entire system (see Figure 2), minimizing time lag and ensuring maximum efficiency. An Arduino Mega operates as the microcontroller, coordinating the activation and deactivation of the EPMS, while a computer is utilized to transmit control commands to the microcontroller. This setup provides a systematic and synchronized approach to control the states of the EPMS in the soft robot. The commercially available motor drivers (BTS7960) are employed for this purpose. They have the capability to send current pulses in both directions at specific times, as directed by input from the microcontroller. The motor drivers operate on 12 V power supplies.

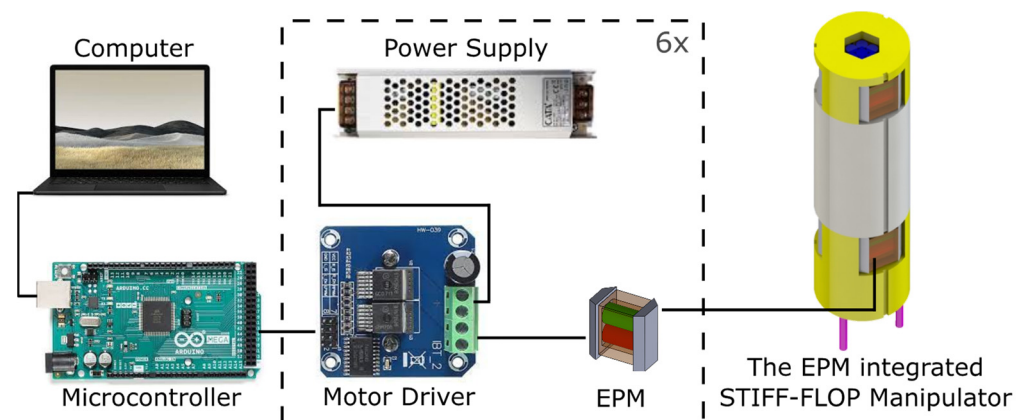


Figure 2. A schematic representation of the control unit of the variable stiffness device.

2.2. Proof-of-Concept Test Setup for the Jamming of MRE Fibers

A proof-of-concept test setup was developed to thoroughly investigate the stiffness change caused by the magnetic jamming of MRE fibers. The setup consists of a fiber jamming structure embedded in the STIFF-FLOP manipulator. The structure contains MRE fibers covered by a flexible sleeve made of NdFeB particles. Two sets of sleeves were manufactured: a non-magnetic sleeve with non-magnetized NdFeB particles, and a magnetic sleeve with magnetized NdFeB particles. The non-magnetic sleeve is used to induce the condition where the MRE fibers are not jammed while the magnetic sleeve is used to jam the MRE fibers. The proof-of-concept test setup is shown in Figure 3. The fiber jamming structure possesses a length of 50 mm and a diameter of 6.5 mm, with a flexible sleeve having a wall thickness of 1 mm. Two different fiber jamming structures were designed to be added to the stiffening chamber of the manipulator, separately. The first structure utilizes one piece of a MRE to observe the stiffness gain caused solely by the MR effect. The second structure is designed with the optimal packing of congruent pieces, which is described in [59] and presents the best packing densities of circles within a circle. Due to manufacturing limitations, the structure is comprised of seven MRE fibers. The

MRE fibers are shown in Figure 3. The diameter of the MRE piece is 1.5 mm and the seven fibers have a diameter of 4.5 mm.

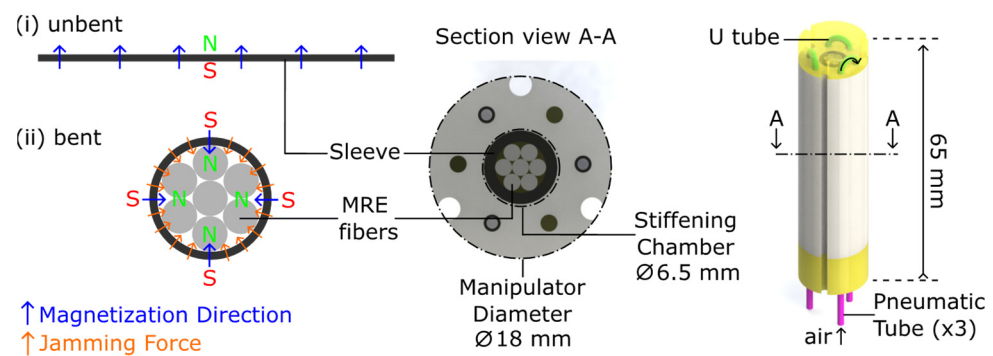


Figure 3. Proof-of-concept test setup. (Left) Conceptual design of the fiber jamming structure. The magnetic polarization of the sleeve with magnetized NdFeB particles changes to a radial direction when the magnet is bent. (Middle) A cross-sectional view of the manipulator shows the densely packed MRE fibers and the sleeve within the stiffening chamber. (Right) CAD drawing of the fiber-jamming-structure-integrated STIFF-FLOP manipulator.

2.3. Fabrication

The MRE samples used in the experiments were fabricated using Ecoflex 00-30 (Smooth-On Inc., Macungie, PA, USA) as an elastomer matrix and 5 μm of carbonyl iron particles (CIPs). The matrix material is comprised of two components: Part A and the hardener component Part B. Initially, Part A and CIPs were mixed to facilitate the fabrication process. Subsequently, Part B was thoroughly mixed into the homogenous mixture until all ingredients were evenly distributed. The mixture was placed into a vacuum chamber for 3 min at -1 bar to ensure proper elimination of air bubbles. It was then poured into 3D-printed PLA molds and the curing process was performed at room temperature for four hours. MRE samples with a volume fraction of 30% ($f = 0.3$) were prepared for conducting the experiments. The size of the samples used in the tests was 50 mm in length. The diameters of the fibers used in the fiber jamming structure were 4.5 mm and 1.5 mm; meanwhile, they were 2.2 mm and 1.34 mm for variable stiffness devices.

The EPM device is composed of a rigid NdFeB magnet, an AlNiCo magnet, two steel caps, and a copper wire. The N42 grade NdFeB magnets and the AlNiCo 5 magnets were purchased from KJ Magnetic, Inc. and McMaster-Carr, respectively. The diameter and the length of the magnets were 3.18 mm and 6.35 mm, respectively. The magnets were glued to the caps using an epoxy adhesive and wrapped with a coil of 80 turns of 28 AWG copper wire.

Fabrication of the STIFF-FLOP manipulator required several silicone molding steps. The fabrication process of the manipulator can be seen in Figure 4. First, the chamber molds were threaded with an inextensible polyester thread around a 3D-printed cylinder. The cylinder is made up of three parts: an inner core and two side parts. Six molds were placed in a module mold, as shown in Figure 4a. In this way, the radial expansion of the chamber was prevented. The mold was filled with uncured silicone (Ecoflex 00-50, Smooth-On) and left to cure at room temperature [see Figure 4b(i)]. The chamber molds were removed after the silicone had completely cured, beginning with the core and then sliding out the other two side parts. This disassembly of the chamber molds allowed them to be loosened within the cured body, allowing easier removal while keeping the thread in place. Second, another layer of silicone was applied to the inside of the chambers to integrate the thread within the body. In order to complete the second layer process, the thin rods (core) with a diameter of 2 mm were inserted into the chamber. The second curing step was, thus, performed by pouring the same uncured silicone into the remaining free space of the side parts, as shown in Figure 4b(ii). Then, the U-shaped Polyvinyl chloride (PVC) tubes with an inner diameter of 1.5 mm and an outer diameter of 2 mm were placed in the fluidic chamber, as depicted in Figure 4b(iii). They were used to connect the double chambers.

The third curing step involved pouring the same uncured silicone into the remaining free space within the module mold.

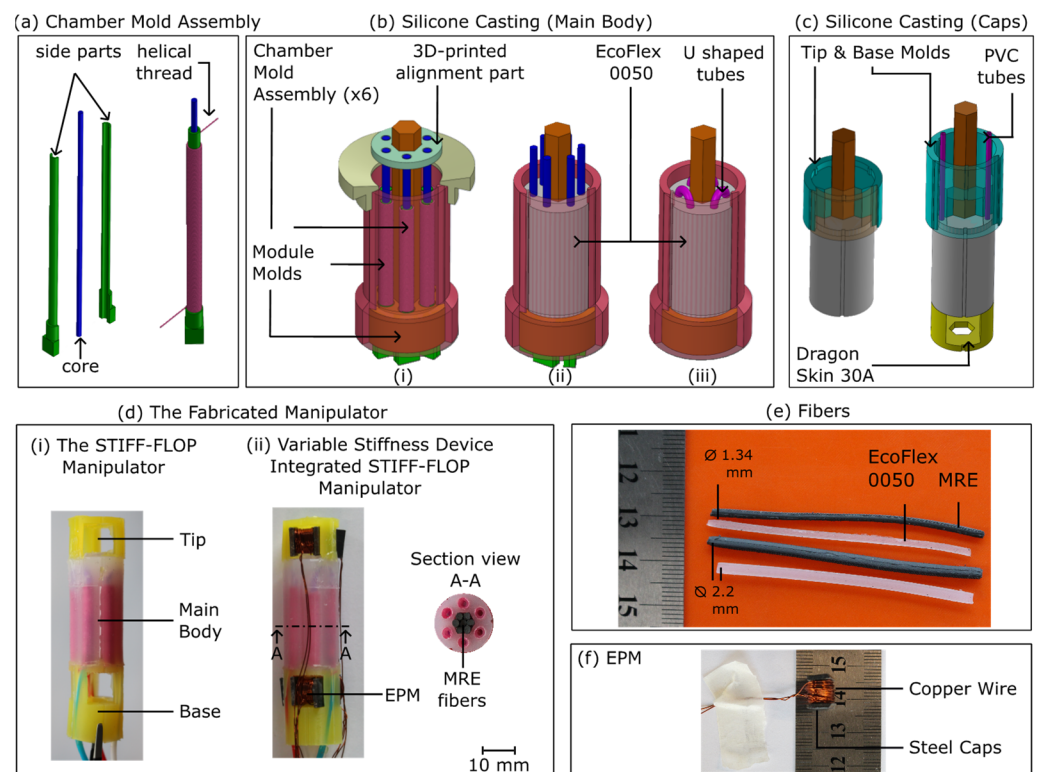


Figure 4. Fabrication of the STIFF-FLOP manipulator with the proposed variable stiffness device. (a) The 3D-printed side parts and a core are assembled; then, polyester is wound around the mold. (b) The silicone casting steps (i–iii) of the body of the manipulator. (c) Fiber jamming structures are inserted; then, the top and bottom ends are sealed to the body. (d) Images of (i) the fabricated STIFF-FLOP manipulator and (ii) the variable stiffness device implemented version. (e) The fibers and (f) an EPM.

Third, the main body of the manipulator is sealed at the top and bottom caps with hard silicone (DragonSkin 30A, Smooth-On), as depicted in Figure 4c. Additionally, an adhesive (Sil-Poxy, Smooth-On) was applied to three of the air channels and PVC tubes were used in the remaining channels to prevent hard silicone from blocking the air channels. Finally, the MRE fibers were inserted into the corresponding positions with the help of a 3D-printed part encapsulating the fibers. Then, the EPM devices (in the OFF state) were placed in the corresponding positions at the final stage. Figure 4d shows the STIFF-FLOP manipulator with the variable stiffness device. The molds used in the fabrication were disposable and manufactured using a 3D printer (Bambu Lab X1-Carbon). Three manipulators were fabricated to demonstrate their reproducibility for use in stiffening tests. The fabricated parts of the variable stiffness device are shown in Figure 4e,f.

Flexible sleeves that are used in the proof-of-concept test setup were manufactured to provide both jamming force and a magnetic field to the MRE fibers (see Figure 5a). The elastomer of the sleeve was PDMS (Sylgard 184, Dow Corning Inc.) loaded with neodymium-iron-boron (NdFeB) microparticles (QP-S-11-9-20001, Magnequench, Co. Ltd., Tianjin, China, density: 7.43 g/cm^3) in a mass ratio of 10:1 (mass of NdFeB microparticles to the mass of PDMS). The fabrication methods used for MRE fiber production were applied to the production of the flexible sleeve as well. Half of the manufactured flexible sleeves were exposed to a large uniform magnetic field of 2.1 T using a dipole electromagnet (5403AC, GMW Associates) to obtain magnetic sleeves. The length, width, and thickness of the magnets were 50 mm, 20 mm, and 1 mm, respectively. Magnetic field measurements were

carried out using a Tesla meter (PCE-MFM 2400). The magnetic properties of the sleeve were provided directly by the manufacturer and were calculated based on an estimation using the volumetric loading of magnetic powder. The retentivity and coercivity values were set at 447 mT and 296 kA/m (H_c), respectively.

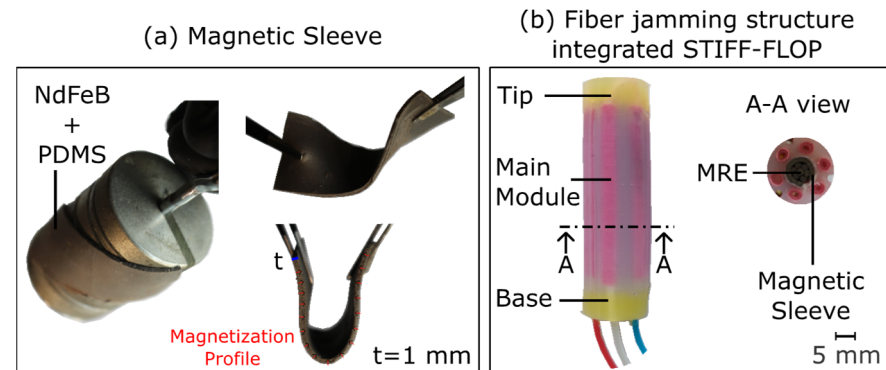


Figure 5. Fabrication of the fiber jamming structure. (a) Images of a flexible magnetic sleeve made of NdFeB microparticles and PDMS. (b) The fiber jamming structure is integrated into the STIFF-FLOP manipulator.

The fabrication process for the STIFF-FLOP manipulator with the integrated fiber jamming structure closely followed the same steps, with the only difference being the insertion of the structure into the stiffening chamber before casting the tip and base of the manipulator. Additionally, Parafilm tape was placed at the ends of the fibers before casting the tip and base of the manipulator to protect against potential leakage. Twelve manipulators were manufactured to perform stiffening tests, encompassing four cases: combinations of two sets of sleeves and two different numbers of fibers in the stiffening chamber. For each case, three manipulators were manufactured to highlight the reproducibility.

2.4. Modeling

A 3D model with identical dimensions and magnetic properties to the physical model has been constructed using the Maxwell 3D module in ANSYS. The model consists of three radially oriented EPMS, seven MRE fibers, and a surrounding region. An EPM is composed of an AlNiCo magnet, a NdFeB magnet, two steel caps, and a copper region. The N42 grade NdFeB magnet ($B_r = 1.23$ T) and AlNiCo 5 ($B_r = 1.26$ T) magnet were used in the simulation. The diameter and length of the magnets were 3.18 mm and 6.35 mm, respectively. The magnets were enclosed with the copper region. The pole directions of the magnets were adjusted as illustrated in the model. Specifically, the pole directions of the magnet pairs were set to differ by 120 degrees from each other. The MRE fibers were modeled with a relative permeability based on [43]. The surrounding vacuum domain was modeled as a rectangular prism with a 100% offset in the $-x$, $-y$, and $-z$ directions. The meshing process utilized automatic adaptive meshing, employing a total of 65,000 elements. The number of passes within the simulations was set at 10, with an energy error of 1%. The simulations were conducted for all EPMS in their ON and OFF states.

Two simulations were conducted on the model. First, a magnetic jamming force created by an individual EPM was simulated by selecting components, including the magnets, the caps, and the copper region. Second, a simulation was performed to calculate the magnetic flux density passing through the MRE fibers. In addition, to validate the accuracy of the simulations, magnetic measurements were taken using the Tesla meter from the center of the caps of the EPM pairs that were oriented toward each other. These measurements were conducted repeatedly at distances d of 3 mm, 2.5 mm, and 1 mm. Furthermore, magnetic simulations were conducted for scenarios involving distances (0.5 mm and 0.1 mm) where measurements could not be taken due to geometric limitations.

Assuming the hard and the soft magnets within the EPM are fully magnetized in the same direction and there is no gap between the caps and the target object, magnetic force can be theoretically calculated. The formula for determining the magnetic force exerted by an EPM is expressed as:

$$F = \frac{1}{\mu_0 ab} \left(\frac{\pi B_r d_m^2 N_{rods}}{4} \right)^2 \tag{3}$$

where F represents the magnetic force; d_m is the diameter of the magnets; N_{rods} is the number of magnets within the EPM, which is two; μ_0 is the permeability of free space; and a (10 mm) and b (1.5 mm) are the width and thickness of the caps, respectively. The equation was retrieved from [60].

The measurement and simulation results are presented in Figure 6. It can be inferred from Figure 6e that the simulation results match the magnetic measurements. An exponential regression is employed to model the resulting magnetic simulation force data, offering a forecast of exponential relationships between variables. The magnetic jamming force generated by an EPM is calculated to be 8.39 N when $d = 0.1$ mm. Analytically, the magnetic jamming force is determined to be 20.12 N when $d = 0$ mm. The outcomes indicate that the regression aligns closely with the analytical equation when d is approximately 0.049 mm, a value very close to zero. Considering that the EPMs jam the MRE fibers from their tangential surfaces (note: the contact area is calculated from the CAD drawing to be 3 mm × 10 mm), the magnetic pressure is determined to be 670 kPa. The EPMs produce a mean magnetic field of 0.25 mT in the OFF state and 20.1 mT in the ON state.

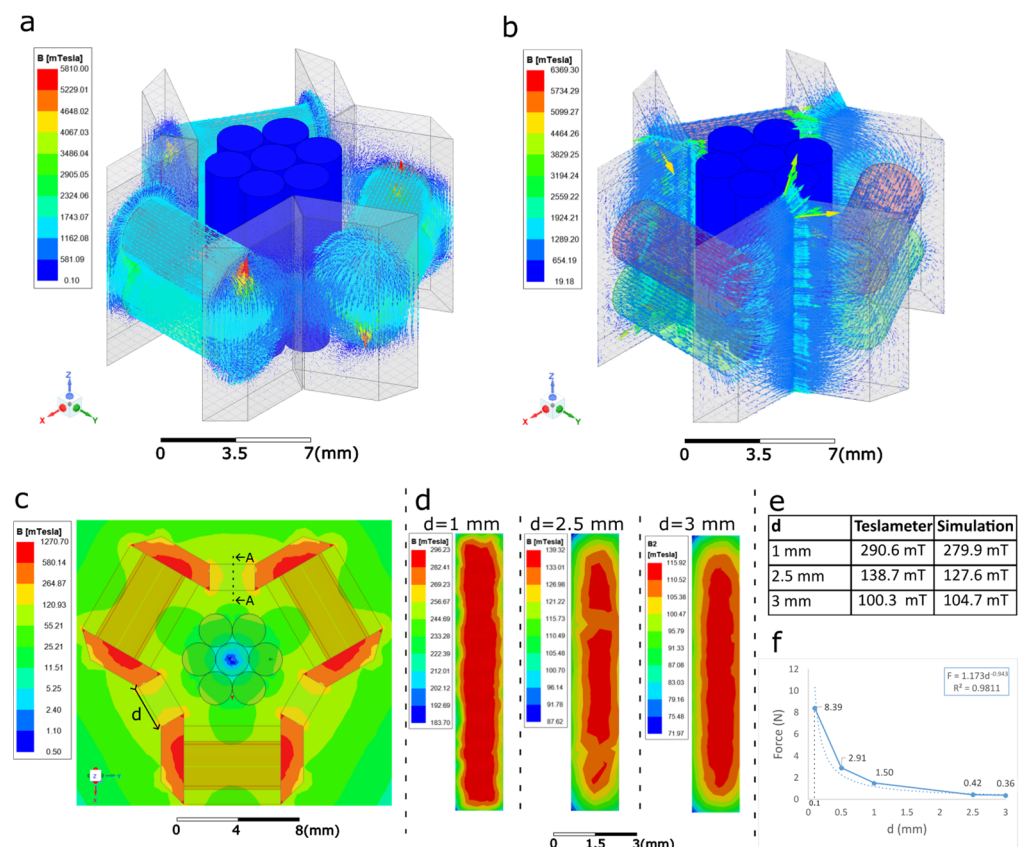


Figure 6. Magnetic simulations of the three EPMs and MRE fibers enclosed in the jamming region. Magnetic field lines when EPMs are in ON states (a) and OFF states (b). (c) Top view of the model, indicating magnetic flux density passing through the MRE fibers when the distance d is 3 mm. (d) Magnetic flux density of the cross-sectional area for each d . (e) Results of the magnetic measurements vs. simulations. (f) Magnetic jamming force produced by an EPM vs. the cap distance d .

3. Experimental Evaluation

Two sets of experiments were conducted to assess the stiffening capabilities of the proposed designs described in Section 2. The proof-of-concept test setup and the variable-stiffness-device-integrated STIFF-FLOP manipulator were tested under two scenarios: magnetically OFF and ON states. In the ON-state experiments, the actuation mechanisms were activated to evaluate the increase in stiffness resulting from the proposed hybrid stiffening method. We investigated both the MR effect, whose working principle relies on the intrinsic properties of MREs, and the jamming effect, which is achieved through kinematic and frictional interactions between the fibers. In the OFF-state experiments, the objective was to determine the base stiffness state, disregarding any changes in stiffness caused by either the MR effect or the jamming effect. The tests were carried out in the base condition, with no actuation in the fluidic chambers.

3.1. Proof-of-Concept Magnetic Fiber Jamming Tests

The experiments were conducted with the fiber jamming structure-integrated manipulators using unmagnetized flexible sleeves in the OFF state and magnetized sleeves in the ON state. Stiffening tests were performed in two deformation modes (bending vs. compression) and with two different numbers of MRE fibers (N is either one or seven). First, a cantilever bending test was conducted on the manipulator, deflecting the tip to measure the change in stiffness. Second, a compression test setup was conducted and the manipulator was strained in the longitudinal direction. Both tests were performed with the fiber jamming structure having one piece of a MRE fiber ($N = 1$) and seven MRE fibers ($N = 7$). Additionally, the tests were carried out on three separate manipulators to demonstrate the repeatability of the results. Each test was repeated five times for statistical purposes. In total 120 trials were performed.

The schematic of the experimental setup can be seen in Figure 7a,d. The setup includes a force measuring unit equipped with a 3 kg miniature load cell, a micrometer screw gauge with a resolution of 0.01 mm, and a stepper motor. During the stiffening experiments, the base of the STIFF-FLOP manipulators was clamped using 3D-printed parts and the tip was left free. In compression tests, the manipulator was tested up to 10% engineering strain using the stepper motor running at a constant rotational speed corresponding to 0.1 mm/s compression speed; meanwhile, it was deflected by 10 mm at a constant speed of 0.2 mm/s in the cantilever bending tests. The resulting force was measured by the load cell and the tests were displacement controlled.

The results of the compression tests of the fiber jamming structure are shown in Figure 7b,c. The results indicate that the resultant stress (calculated by dividing the resultant force by the initial cross-sectional area of the manipulator) upon loading shows a nearly linear behavior with strain for each case ($R^2 \geq 0.9960$). The slopes of the stress vs. strain curves upon loading are assumed to give compression modulus values of the fiber jamming structures. It can be inferred from the figures that the compression modulus increases when the magnetized sleeves are used in the structure. The modulus of the OFF-state structure is calculated as 394.9 kPa when $N = 1$ while the ON-state modulus is calculated as 436.8 kPa. In addition, the results indicate that the compression modulus decreases with increasing N . For example, the modulus of the unjammed structure is calculated as 394.9 kPa when $N = 1$ while it is 378.4 kPa when $N = 7$.

The results of the cantilever bending tests of the fiber jamming structure are shown in Figure 7e,f. The stress–strain curves exhibited a highly noticeable hysteresis behavior. The area between the curves signifies the amount of dissipated energy. The slope of the force vs. displacement curves upon loading gives the bending stiffness value of the fiber jamming structure. The results indicate that the resulting stiffness increases when the magnetized sleeves are used in the jamming structure. For instance, the OFF-state stiffness of the structure with a single piece of a MRE is calculated as 0.39 N/cm while the ON-state stiffness is calculated as 0.43 N/cm in the cantilever bending tests. In addition,

the corresponding increase is also observed when $N = 7$. The stiffness is increased from 0.33 N/cm to 0.40 N/cm.

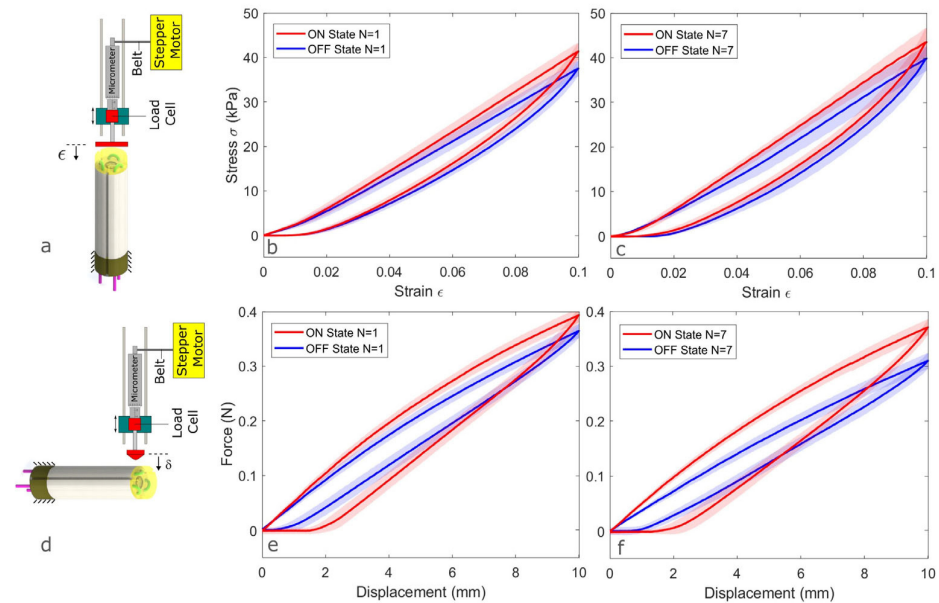


Figure 7. (a,d) Schematics of the compression and cantilever bending test setup, respectively. Compression test results of the structure-integrated STIFF-FLOP manipulators are indicated in (b) when the number of MRE fibers $N = 1$ and in (c) when $N = 7$. The same manipulators were tested in the cantilever bending tests. Results are shown in (e,f) for the number of MRE fibers $N = 1$ and $N = 7$, respectively. Solid lines show the mean of all tests and the shaded area indicates the standard error of the mean.

In addition to the presented stiffness values for the fiber jamming structures, the stiffness ratio (K , the ratio of jammed stiffness to unjammed stiffness) is calculated as well. The cantilever bending results show that K increases with increasing N . K is 1.1 when $N = 1$ while it is 1.21 when $N = 7$. As for compression tests, the change in modulus is calculated as 1.11 for each case. Considering the fact that axially oriented fibers in a jamming structure have no effect on stiffness change under compression, the change in stiffness can be considered due to the MR effect. The optimal stiffness change of the structure is observed when $N = 7$. We observed a 21.2% increase in the stiffness variation of the structure.

3.2. Electronically Controlled Variable Stiffness Tests

To demonstrate the variable stiffness device’s ability to stiffen, we conducted cantilever bending experiments using the device-integrated STIFF-FLOP manipulator. Our tests considered three experimental factors: two operating modes of the EPMs (ON or OFF), two materials for the fibers (pure silicone or MRE), and the number of MRE fibers (either seven or nineteen). The cantilever bending test results are shown in Figure 8. The bending stiffness values of the manipulator are determined by analyzing the slopes of the resulting loading force versus the deflection curve. Stiffness for each case is computed through a linear fit ($R^2 \geq 0.9938$) across the entire loading range. The results indicate that the stiffness of the jammed manipulators is higher than that of unjammed ones. This aligns with expectations as the EPMs create both magnetic fields and jamming forces, collectively augmenting the overall stiffness of the manipulator. Additionally, the results demonstrate a decrease in manipulator stiffness with an increase in the number of fibers utilized within the variable stiffness device. For instance, when employing MRE fibers where $N = 7$, the stiffness values for unjammed and jammed manipulators are calculated as 0.39 N/cm and 0.45 N/cm, respectively. The values are decreased to 0.34 N/cm and 0.42 N/cm, correspondingly, when $N = 19$. The results revealed that using more fibers in the device

raises the K value. For instance, with pure silicone fibers (Ecoflex 00-30), the K value is 1.12 when $N = 7$; however, this rises to 1.17 when $N = 19$. Similarly, adding MRE fibers increases stiffness, with corresponding K values of 1.17 and 1.23 when $N = 7$ and $N = 19$, respectively.

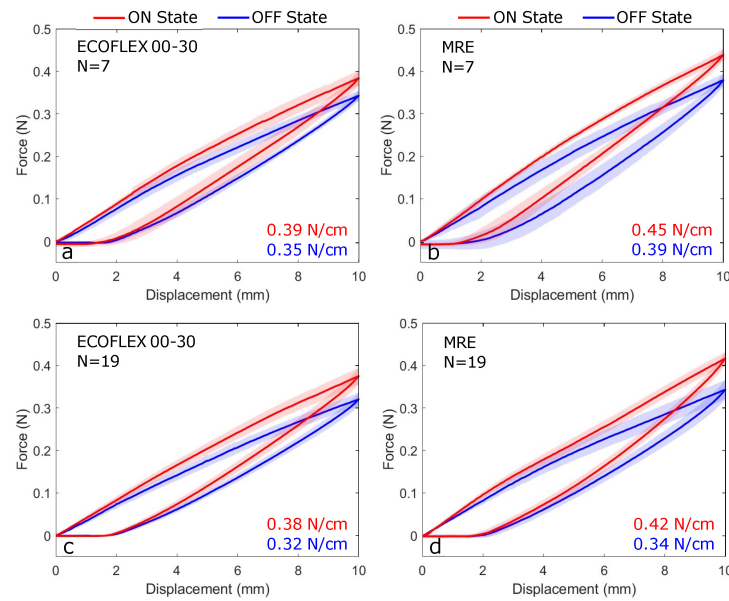


Figure 8. Cantilever bending test results of the stiffening-device-integrated STIFF-FLOP manipulator. Force vs. deflection curves in (a,b) and (c,d) represent the results when the number of fibers are $N = 7$ and $N = 19$, respectively. Corresponding stiffness values are indicated at the bottom right of the subfigures.

3.3. Bending Angle Tests

The bending angle of the manipulator was assessed in two configurations: magnetic (ON state) and non-magnetic (OFF state), employing the proposed variable-stiffness-device-integrated STIFF-FLOP with 19 MRE fibers (see Video S2). To calculate the bending angle, a video capturing the manipulator carrying a 20 g weight at the tip was recorded from a front-view perspective. This video was further processed using the vector graphics software Inkscape, 1.2.1. An algorithm was employed to analyze the final captured image, determining the bending angle. An imaginary line drawn on the tip served as a reference and the angle between this line and the vertical axis indicated the bending angle. The tests were repeated five times for each configuration. The captured images shared identical aspect ratios and pixel counts. The results of the bending angle tests are shown in Figure 9. The results indicate that the bending angle is decreased from 12.74 (deg) to 10.07 (deg), resulting in a 20.97% change when the magnetic state of the EPMS within the variable stiffness device is switched from the OFF to ON state.

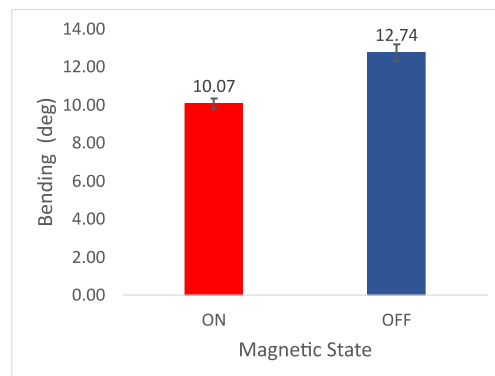


Figure 9. Bending angle results of the STIFF-FLOP manipulator with the variable stiffness device.

4. Discussion

The primary rationale of this study is to investigate the jamming behavior of MRE fibers to leverage both the alteration in the viscoelasticity characteristic of MREs under a magnetic field and an increase in the magnetic jamming force. The changes in stiffness can be attributed to two key factors: the jamming effect and the MR effect. In our experiments, we conducted tests using a non-magnetic material—pure silicone (Ecoflex 00-30) fibers—in the variable stiffness device. This approach allowed us to eliminate the MR effect and solely examine the impact of jamming. The outcomes obtained from the variable stiffness device affirm that the proposed design is more effective when employing MREs instead of the Ecoflex 00-30, emphasizing the advantage of incorporating MREs in the system. For instance, when $N = 7$, the stiffness increase in the manipulator with the Ecoflex 00-30 and MRE fibers is calculated at 11.53% and 13.23%, respectively, resulting in a 1.70% difference. Meanwhile, when $N = 19$, this discrepancy is calculated as 5.90%. Additionally, the MR effect achieved through the variable stiffness device is comparatively lower than that observed in the fiber jamming structure. This discrepancy arises because the jamming is induced discretely, occurring solely in the base and tip regions. The magnetic fields supplied by the EPMs cover only two-fifths of the fiber region, limiting the extent of the MR effect generated within the device. Moreover, we have showcased an alternate approach to implementing a magnetically driven jamming technique, offering a rapid response time and requiring reduced energy consumption compared to the current pneumatic jamming method. The proposed actuation mechanism exhibits a response time of 100 μs and consumes an estimated 49.92 mJ of energy, as outlined in the calculations provided in Appendix A.

In the proof-of-concept magnetic fiber jamming tests, the jamming is induced continuously and the flexible sleeve supplies magnetic fields throughout the fibers' entire length. We observed a noticeable increase in stiffness change due to both the MR effect and the jamming effect. Our estimation suggests that these approaches contributed almost equally to the overall effect. Specifically, we observed a consistent 11% increase in stiffness during compression mode due to the MR effect, regardless of the fiber count within the structure. This percentage escalated to 21.2% in the bending test, owing to the combined hybrid effect of both mechanisms. The resulting stiffness change theoretically should have been $K = 8.61$ for $N = 7$, [16]. However, we obtained $K = 1.21$ from the experiments. This deviation primarily results from a substantial portion of unjammed material present within the manipulator. Specifically, the diameter of the jammed region measures 4.5 mm (excluding the sleeve thickness) while the overall manipulator diameter spans 18 mm.

5. Conclusions

In this study, a novel variable stiffness device combining jamming with viscoelasticity modification has been developed to achieve stiffness modification. The proposed device is innovative as it utilizes the benefits of magnetic jamming in MREs to enhance stiffness variation. We demonstrated the increase in stiffness by utilizing this hybrid method in the STIFF-FLOP manipulator under different deformation modes. The results indicate that the proposed hybrid stiffening method is promising for achieving variable and controllable stiffness in soft robots.

We investigated the behavior of the magnetically induced jamming of MRE fibers as a first step toward a hybrid variable stiffness method. The fiber jamming structure consisting of MRE fibers and a flexible sleeve was implemented on the STIFF-FLOP manipulator. The stiffening tests were performed on the device-integrated manipulator. The tests were repeated with the magnetized and unmagnetized sleeves to explore the stiffness change. The manipulator achieved stiffness variation under different deformation modes, such as bending and compression.

The originality of this work is based on the development of a novel variable stiffness device utilizing two stiffening methods: a jamming-based method and a viscosity-based method. The device comprises MRE fibers and EPMs, compactly positioned within the

manipulator's stiffening chamber. Stiffening tests were conducted on the device-integrated STIFF-FLOP manipulator to assess its ability to enhance stiffness. The outcomes obtained from the variable stiffness device confirm that the device exhibits greater effectiveness when utilizing MREs rather than pure silicone. Additionally, the incorporation of EPMS offers rapid jamming transitions, leading to reduced energy consumption.

The stiffening method proposed in this study has the potential to achieve a high range of stiffness variation, a fast response time, and suitability for different modes when implemented in a soft manipulator. With this device, it is also possible to obtain various stiffening states. In the softest state, the six EPMS are in the OFF state; whereas, the rigid state is obtained when the EPMS are switched to the ON state. Different stiffness states can be obtained between the maximum and minimum values depending on the number of activated EPMS and the configuration. Furthermore, the hybrid methodology utilized in this study exhibits potential for application in diverse industrial scenarios where rapid and energy-efficient transitions are requisite for variable stiffness requirements.

The response of the manipulator to the applied magnetic jamming force is notably complex. The variable stiffness device consists of MRE fibers and EPMS at both the base and tip, delivering discrete magnetic jamming forces. Furthermore, the device is embedded within the manipulator's central channel, contributing to its complexity. The manipulator comprises three soft materials (MRE, Ecoflex 00-50, and Dragon Skin 30A) and three rigid materials (NdFeB, AlNiCo, and steel). Due to this intricate geometry and material composition, a comprehensive analysis involving complex mathematical equations or multi-physics finite element analysis is needed. This aspect is a potential avenue for future investigation.

There exists sufficient space for additional enhancements in the proposed device. First, the high permeability of the magnetic particles can be incorporated into the elastomer matrix to maximize the MR effect. Second, employing advanced manufacturing methods like micro-molding and extrusion-based 3D printing can reduce the diameter of MRE fibers in the variable stiffness device. Consequently, this allows for a greater number of fibers to be stacked within the device. Third, there is potential for optimizing the geometry of the manipulator without compromising its performance. Enhancements could focus on adjusting the ratio between the jammed and unjammed regions without impeding the robot's capabilities. Finally, six EPMS, which account for almost half of the manipulator's weight, provide discrete jamming in this study. However, the design can be further developed to provide continuous jamming, aiming to reduce the number of EPMS used in the manipulator. Because most of the soft robotic tasks are performed in cylindrical coordinates, there is a demand for novel EPM designs that facilitate jamming in the radial direction. Achieving this would involve utilizing magnets featuring radial magnetic polarization and optimizing the cap geometry of the EPMS.

Supplementary Materials: The following supporting information can be downloaded at: <https://www.mdpi.com/article/10.3390/robotics13010016/s1>, Video S1: Jamming of the MRE fibers utilizing the EPMS. Video S2: Bending of the STIFF-FLOP manipulator with the variable stiffness device. Video S3: Variable-stiffness-device-integrated STIFF-FLOP manipulator.

Author Contributions: Conceptualization, T.A. and E.S.; methodology, T.A., F.K. and E.S.; software, T.A.; validation, T.A., F.K. and E.S.; formal analysis, T.A.; investigation, T.A.; resources, T.A., N.P., M.C. and E.S.; data curation, T.A.; writing—original draft preparation, T.A. and E.S.; writing—review and editing, T.A., F.K., N.P., M.C. and E.S.; visualization, T.A.; supervision, E.S.; project administration, E.S.; funding acquisition, M.C. and E.S. All authors have read and agreed to the published version of the manuscript.

Funding: This project was in part supported by the Boğaziçi University Research Fund, grant numbers 17641 and 19782. The research leading to these results has received funding from the European Union's Horizon 2020 Research and Innovation Program under grant agreement No. 730994 (TERRINet). We also acknowledge the support received from the Boğaziçi University Robotics

and AI Laboratories Project (ROYAL), funded by the Presidency of Strategy and Budget of the Republic of Türkiye.

Data Availability Statement: Data are available upon request.

Acknowledgments: We would like to thank Günay Züngör, who contributed to the preparation of the experiment setup, and Emre Özgül, who contributed to the fabrication of the STIFF-FLOP manipulator and the Supplementary Video.

Conflicts of Interest: The authors declare no conflicts of interest.

Abbreviations

The following abbreviations are used in this manuscript:

CIP	Carbonyl Iron Particle
EPM	Electro-permanent magnet
FFA	Flexible Fluidic Actuator
MIS	Minimally Invasive Surgery
MR	Magnetorheological
MRE	Magnetorheological Elastomers

Appendix A

An EPM consists of two permanent magnets (a hard and a soft magnet), metal caps, and a coil. The target surface and the caps are separated by an air gap, which is denoted as g . The soft and hard magnets have almost the same remanent magnetization; however, they have different coercivity values. The hard magnet has a very high coercivity; whereas, the coercivity value of the soft magnet is relatively low. The magnets have the same length (L_m) and diameter (d_m). The caps and coil are made from iron and copper, respectively. The working principle of an EPM device in operation can be seen in Figure A1. The directions of the current and magnetic flux in the EPM device are illustrated as orange and cyan arrows, respectively. The switching current flows through the coil and the soft magnet is magnetized up to a saturation point. A part of the flux flows through the target surface (illustrated by cyan dotted lines); however, the majority of the flux device goes through the EPM device. When the soft magnet is fully saturated, the switching current is turned off, i.e., the magnetic field intensity is reduced to zero. However, the magnetic flux density is equal to the remanent magnetism. The remanence (i.e., retentivity) value is almost the same for the hard and soft magnet in the ON state. When switching to the OFF state, the current is turned on in the opposite direction. The soft magnet is demagnetized up to the point of full saturation but, this time, in the third quadrant of the B-H curve. The polarity of the soft magnet is changed. When the soft magnet reaches full saturation, the switching current is turned off again. The magnetic flux density is equal to negative remanent magnetism. In the OFF state, magnetic flux flows only through the magnets.

The EPM's resistance is measured to be 1.5Ω and the inductance is calculated analytically as $20.1 \mu\text{H}$ from Equation (A1), where L_{coil} is inductance, μ_0 is vacuum magnetic permeability, N is the number of turns, r is the radius of a magnet, and L_m is the length of the magnet. The pulse time of the current applied is $100 \mu\text{s}$. The energy consumption to change the state of an EPM is calculated as 8.32 mJ from Equation (A2), where R_{coil} is resistance, L_{coil} is inductance, and t is the pulse time. The equations are retrieved from [61]:

$$L_{coil} = \frac{2\pi\mu_0(Nr)^2}{L_m} \quad (\text{A1})$$

$$E = \frac{V^2}{R_{coil}} \left\{ t + \frac{L_{coil}}{R_{coil}} \left[\left(e^{-R_{coil}t/L_{coil}} \right) - 1 \right] \right\} \quad (\text{A2})$$

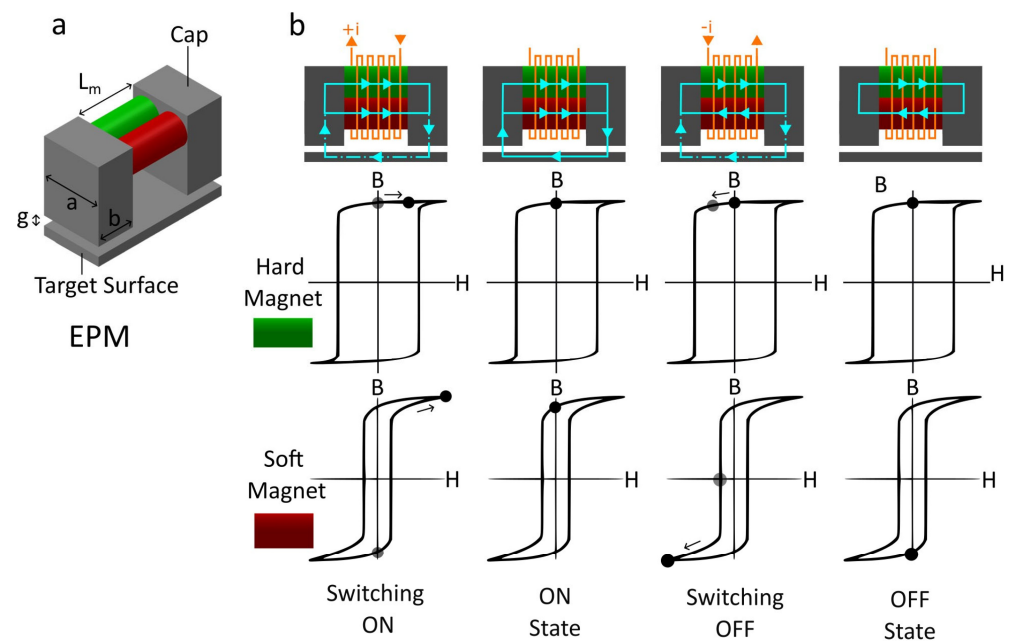


Figure A1. The operation principle of the EPM device. (a) An EPM device. (b) The operation states and corresponding B–H curves of the soft and the hard magnets.

References

1. Trivedi, D.; Rahn, C.D.; Kier, W.M.; Walker, I.D. Soft robotics: Biological inspiration, state of the art, and future research. *Appl. Bionics Biomech.* **2008**, *5*, 99–117. [\[CrossRef\]](#)
2. Majidi, C. Soft robotics: A perspective—Current trends and prospects for the future. *Soft Robot.* **2014**, *1*, 5–11. [\[CrossRef\]](#)
3. Manti, M.; Cacucciolo, V.; Cianchetti, M. Stiffening in soft robotics: A review of the state of the art. *IEEE Robot. Autom. Mag.* **2016**, *23*, 93–106. [\[CrossRef\]](#)
4. Gong, X.; Xie, F.; Liu, L.; Liu, Y.; Leng, J. Electro-active variable-stiffness corrugated structure based on shape-memory polymer composite. *Polymers* **2020**, *12*, 387. [\[CrossRef\]](#) [\[PubMed\]](#)
5. Frasci, J.; Althoefer, K. A fluidic actuator with an internal stiffening structure inspired by mammalian erectile tissue. In Proceedings of the 2023 IEEE International Conference on Robotics and Automation (ICRA), London, UK, 29 May–2 June 2023; pp. 662–668.
6. Hu, J.; Liu, T.; Zeng, H.; Chua, M.X.; Katupitiya, J.; Wu, L. Static Modeling of a Class of Stiffness-Adjustable Snake-like Robots with Gravity Compensation. *Robotics* **2022**, *12*, 2. [\[CrossRef\]](#)
7. Mawah, S.C.; Park, Y.J. Tendon-Driven Variable-Stiffness Pneumatic Soft Gripper Robot. *Robotics* **2023**, *12*, 128. [\[CrossRef\]](#)
8. Pagliarani, N.; Arleo, L.; Albin, S.; Cianchetti, M. Variable Stiffness Technologies for Soft Robotics: A Comparative Approach for the STIFF-FLOP Manipulator. *Actuators* **2023**, *12*, 96. [\[CrossRef\]](#)
9. Chenal, T.P.; Case, J.C.; Paik, J.; Kramer, R.K. Variable stiffness fabrics with embedded shape memory materials for wearable applications. In Proceedings of the 2014 IEEE/RSJ International Conference on Intelligent Robots and Systems, Chicago, IL, USA, 14–18 September 2014; pp. 2827–2831.
10. Childs, J.A.; Rucker, C. Leveraging geometry to enable high-strength continuum robots. *Front. Robot. AI* **2021**, *8*, 629871. [\[CrossRef\]](#)
11. Sun, Y.; Lueth, T.C. Enhancing Torsional Stiffness of Continuum Robots Using 3-D Topology Optimized Flexure Joints. *IEEE/ASME Trans. Mechatron.* **2023**, *28*, 1844–1852. [\[CrossRef\]](#)
12. Fitzgerald, S.G.; Delaney, G.W.; Howard, D. A review of jamming actuation in soft robotics. *Actuators* **2020**, *9*, 104. [\[CrossRef\]](#)
13. Liu, A.J.; Nagel, S.R. Jamming is not just cool any more. *Nature* **1998**, *396*, 21–22. [\[CrossRef\]](#)
14. van Hecke, M. Jamming of soft particles: Geometry, mechanics, scaling and isotaticity. *J. Phys. Condens. Matter* **2009**, *22*, 033101. [\[CrossRef\]](#)
15. Bi, D.; Zhang, J.; Chakraborty, B.; Behringer, R.P. Jamming by shear. *Nature* **2011**, *480*, 355–358. [\[CrossRef\]](#)
16. Aktaş, B.; Narang, Y.S.; Vasios, N.; Bertoldi, K.; Howe, R.D. A modeling framework for jamming structures. *Adv. Funct. Mater.* **2021**, *31*, 2007554. [\[CrossRef\]](#)
17. Zhou, Y.; Headings, L.M.; Dapino, M.J. Discrete layer jamming for variable stiffness co-robot arms. *J. Mech. Robot.* **2020**, *12*, 015001. [\[CrossRef\]](#)
18. Jiang, Y.; Chen, D.; Liu, C.; Li, J. Chain-like granular jamming: A novel stiffness-programmable mechanism for soft robotics. *Soft Robot.* **2019**, *6*, 118–132. [\[CrossRef\]](#)

19. Tanaka, K.; Karimi, M.A.; Busque, B.P.; Mulroy, D.; Zhou, Q.; Batra, R.; Srivastava, A.; Jaeger, H.M.; Spenko, M. Cable-driven jamming of a boundary constrained soft robot. In Proceedings of the 2020 3rd IEEE International Conference on Soft Robotics (RoboSoft), New Haven, CT, USA, 15 May–15 July 2020; pp. 852–857.
20. Santiago, J.L.C.; Godage, I.S.; Gonthina, P.; Walker, I.D. Soft robots and kangaroo tails: Modulating compliance in continuum structures through mechanical layer jamming. *Soft Robot.* **2016**, *3*, 54–63. [[CrossRef](#)]
21. Diller, S.B.; Collins, S.H.; Majidi, C. The effects of electroadhesive clutch design parameters on performance characteristics. *J. Intell. Mater. Syst. Struct.* **2018**, *29*, 3804–3828. [[CrossRef](#)]
22. Wang, T.; Zhang, J.; Li, Y.; Hong, J.; Wang, M.Y. Electrostatic layer jamming variable stiffness for soft robotics. *IEEE/ASME Trans. Mechatron.* **2019**, *24*, 424–433. [[CrossRef](#)]
23. Okatani, Y.; Nishida, T.; Tadakuma, K. Development of universal robot gripper using MR α fluid. In Proceedings of the IEEE 2014 Joint 7th International Conference on Soft Computing and Intelligent Systems (SCIS) and 15th International Symposium on Advanced Intelligent Systems (ISIS), Kitakyushu, Japan, 3–6 December 2014; pp. 231–235.
24. Gaeta, L.T.; McDonald, K.J.; Kinnicutt, L.; Le, M.; Wilkinson-Flicker, S.; Jiang, Y.; Atakuru, T.; Samur, E.; Ranzani, T. Magnetically induced stiffening for soft robotics. *Soft Matter* **2023**, *19*, 2623–2636. [[CrossRef](#)] [[PubMed](#)]
25. Brown, E.; Rodenberg, N.; Amend, J.; Mozeika, A.; Steltz, E.; Zakin, M.R.; Lipson, H.; Jaeger, H.M. Universal robotic gripper based on the jamming of granular material. *Proc. Natl. Acad. Sci. USA* **2010**, *107*, 18809–18814. [[CrossRef](#)]
26. Wei, Y.; Chen, Y.; Ren, T.; Chen, Q.; Yan, C.; Yang, Y.; Li, Y. A novel, variable stiffness robotic gripper based on integrated soft actuating and particle jamming. *Soft Robot.* **2016**, *3*, 134–143. [[CrossRef](#)]
27. Cheng, N.G.; Lobovsky, M.B.; Keating, S.J.; Setapen, A.M.; Gero, K.I.; Hosoi, A.E.; Iagnemma, K.D. Design and analysis of a robust, low-cost, highly articulated manipulator enabled by jamming of granular media. In Proceedings of the 2012 IEEE International Conference on Robotics and Automation, Saint Paul, MN, USA, 14–18 May 2012; pp. 4328–4333.
28. Yamane, S.; Wakimoto, S. Development of a flexible manipulator with changing stiffness by granular jamming. In Proceedings of the IEEE 2017 24th International Conference on Mechatronics and Machine Vision in Practice (M2VIP), Auckland, New Zealand, 21–23 November 2017; pp. 1–5.
29. Karimi, M.A.; Alizadehyazdi, V.; Jaeger, H.M.; Spenko, M. A self-reconfigurable variable-stiffness soft robot based on boundary-constrained modular units. *IEEE Trans. Robot.* **2021**, *38*, 810–821. [[CrossRef](#)]
30. Stanley, A.A.; Gwilliam, J.C.; Okamura, A.M. Haptic jamming: A deformable geometry, variable stiffness tactile display using pneumatics and particle jamming. In Proceedings of the IEEE 2013 World Haptics Conference (WHC), Daejeon, Republic of Korea, 14–17 April 2013; pp. 25–30.
31. Baines, R.; Yang, B.; Ramirez, L.A.; Kramer-Bottiglio, R. Kirigami layer jamming. *Extrem. Mech. Lett.* **2023**, *64*, 102084. [[CrossRef](#)]
32. Narang, Y.S.; Aktaş, B.; Ornellas, S.; Vlassak, J.J.; Howe, R.D. Lightweight highly tunable jamming-based composites. *Soft Robot.* **2020**, *7*, 724–735. [[CrossRef](#)]
33. Brancadoro, M.; Manti, M.; Tognarelli, S.; Cianchetti, M. Preliminary experimental study on variable stiffness structures based on fiber jamming for soft robots. In Proceedings of the 2018 IEEE International Conference on Soft Robotics (RoboSoft), Livorno, Italy, 24–28 April 2018; pp. 258–263.
34. Brancadoro, M.; Manti, M.; Grani, F.; Tognarelli, S.; Menciassi, A.; Cianchetti, M. Toward a variable stiffness surgical manipulator based on fiber jamming transition. *Front. Robot. AI* **2019**, *6*, 12. [[CrossRef](#)]
35. Arleo, L.; Lorenzon, L.; Cianchetti, M. Variable stiffness linear actuator based on differential drive fiber jamming. *IEEE Trans. Robot.* **2023**, *39*, 4429–4442. [[CrossRef](#)]
36. Rabinow, J. The magnetic fluid clutch. *Electr. Eng.* **1948**, *67*, 1167. [[CrossRef](#)]
37. Rigbi, Z.; Jilken, L. The response of an elastomer filled with soft ferrite to mechanical and magnetic influences. *J. Magn. Magn. Mater.* **1983**, *37*, 267–276. [[CrossRef](#)]
38. Jolly, M.R.; Carlson, J.D.; Muñoz, B.C.; Bullions, T.A. The magnetoviscoelastic response of elastomer composites consisting of ferrous particles embedded in a polymer matrix. *J. Intell. Mater. Syst. Struct.* **1996**, *7*, 613–622. [[CrossRef](#)]
39. Ginder, J.M.; Nichols, M.E.; Elie, L.D.; Tardiff, J.L. Magnetorheological elastomers: Properties and applications. In Proceedings of the Smart Structures and Materials 1999: Smart Materials Technologies. *SPIE* **1999**, *3675*, 131–138.
40. Bica, I. Compressibility modulus and principal deformations in magneto-rheological elastomer: The effect of the magnetic field. *J. Ind. Eng. Chem.* **2009**, *15*, 773–776. [[CrossRef](#)]
41. Boczkowska, A.; Awietjan, S. Microstructure and properties of magnetorheological elastomers. In *Advanced Elastomers—Technology, Properties and Applications*; InTech: London, UK, 2012; Volume 595. [[CrossRef](#)]
42. Li, W.; Zhang, X.; Du, H. Magnetorheological elastomers and their applications. In *Advances in Elastomers I: Blends and Interpenetrating Networks*; Springer: Berlin, Germany, 2013; pp. 357–374.
43. Schubert, G. Manufacture, Characterisation and Modelling of Magneto-Rheological Elastomers. Ph.D. Thesis, University of Glasgow, Glasgow, UK, 2014.
44. Popp, K.M.; Kröger, M.; Li, W.h.; Zhang, X.Z.; Kosasih, P.B. MRE properties under shear and squeeze modes and applications. *J. Intell. Mater. Syst. Struct.* **2010**, *21*, 1471–1477. [[CrossRef](#)]
45. Li, Y.; Li, J.; Li, W.; Du, H. A state-of-the-art review on magnetorheological elastomer devices. *Smart Mater. Struct.* **2014**, *23*, 123001. [[CrossRef](#)]

46. McDonald, K.; Rendos, A.; Woodman, S.; Brown, K.A.; Ranzani, T. Magnetorheological fluid-based flow control for soft robots. *Adv. Intell. Syst.* **2020**, *2*, 2000139. [[CrossRef](#)]
47. McDonald, K.J.; Kinnicut, L.; Moran, A.M.; Ranzani, T. Modulation of magnetorheological fluid flow in soft robots using electropermanent magnets. *IEEE Robot. Autom. Lett.* **2022**, *7*, 3914–3921. [[CrossRef](#)]
48. Li, Y.; Li, J.; Tian, T.; Li, W. A highly adjustable magnetorheological elastomer base isolator for applications of real-time adaptive control. *Smart Mater. Struct.* **2013**, *22*, 095020. [[CrossRef](#)]
49. Bira, N.; Dhagat, P.; Davidson, J.R. A review of magnetic elastomers and their role in soft robotics. *Front. Robot. AI* **2020**, *7*, 588391. [[CrossRef](#)]
50. Kashima, S.; Miyasaka, F.; Hirata, K. Novel soft actuator using magnetorheological elastomer. *IEEE Trans. Magn.* **2012**, *48*, 1649–1652. [[CrossRef](#)]
51. Kim, J.; Chung, S.E.; Choi, S.E.; Lee, H.; Kim, J.; Kwon, S. Programming magnetic anisotropy in polymeric microactuators. *Nat. Mater.* **2011**, *10*, 747–752. [[CrossRef](#)]
52. Böse, H.; Rabindranath, R.; Ehrlich, J. Soft magnetorheological elastomers as new actuators for valves. *J. Intell. Mater. Syst. Struct.* **2012**, *23*, 989–994. [[CrossRef](#)]
53. Joyee, E.B.; Pan, Y. A fully three-dimensional printed inchworm-inspired soft robot with magnetic actuation. *Soft Robot.* **2019**, *6*, 333–345. [[CrossRef](#)] [[PubMed](#)]
54. Qi, S.; Guo, H.; Fu, J.; Xie, Y.; Zhu, M.; Yu, M. 3D printed shape-programmable magneto-active soft matter for biomimetic applications. *Compos. Sci. Technol.* **2020**, *188*, 107973. [[CrossRef](#)]
55. Hellebrekers, T.; Chang, N.; Chin, K.; Ford, M.J.; Kroemer, O.; Majidi, C. Soft magnetic tactile skin for continuous force and location estimation using neural networks. *IEEE Robot. Autom. Lett.* **2020**, *5*, 3892–3898. [[CrossRef](#)]
56. Kitano, S.; Komatsuzaki, T.; Suzuki, I.; Nogawa, M.; Naito, H.; Tanaka, S. Development of a rigidity tunable flexible joint using magneto-rheological compounds—Toward a multijoint manipulator for laparoscopic surgery. *Front. Robot. AI* **2020**, *7*, 59. [[CrossRef](#)]
57. Cianchetti, M.; Ranzani, T.; Gerboni, G.; De Falco, I.; Laschi, C.; Menciassi, A. STIFF-FLOP surgical manipulator: Mechanical design and experimental characterization of the single module. In Proceedings of the 2013 IEEE/RSJ International Conference on Intelligent Robots and Systems, Tokyo, Japan, 3–7 November 2013; pp. 3576–3581.
58. Abidi, H.; Gerboni, G.; Brancadoro, M.; Frascarelli, J.; Diodato, A.; Cianchetti, M.; Wurdemann, H.; Althoefer, K.; Menciassi, A. Highly dexterous 2-module soft robot for intra-organ navigation in minimally invasive surgery. *Int. J. Med. Robot. Comput. Assist. Surg.* **2018**, *14*, e1875. [[CrossRef](#)]
59. Graham, R.L.; Lubachevsky, B.D.; Nurmela, K.J.; Östergård, P.R. Dense packings of congruent circles in a circle. *Discret. Math.* **1998**, *181*, 139–154. [[CrossRef](#)]
60. Knaian, A.N. Electropermanent Magnetic Connectors and Actuators: Devices and Their Application in Programmable Matter. Ph.D. Thesis, Massachusetts Institute of Technology, Cambridge, MA, USA, 2010.
61. Abeywardana, D.K.; Hu, A.P.; Salcic, Z. Pulse controlled microfluidic actuators with ultra low energy consumption. *Sens. Actuators A Phys.* **2017**, *263*, 8–22. [[CrossRef](#)]

Disclaimer/Publisher’s Note: The statements, opinions and data contained in all publications are solely those of the individual author(s) and contributor(s) and not of MDPI and/or the editor(s). MDPI and/or the editor(s) disclaim responsibility for any injury to people or property resulting from any ideas, methods, instructions or products referred to in the content.